Machine learning based analysis of the Guy-Greenbrier, Arkansas earthquakes: a tale of two sequences

Yongsoo Park[1], S. Mostafa Mousavi[1], Weiqiang Zhu[1], William L. Ellsworth[1], Gregory C. Beroza[1]

[1]Department of Geophysics, Stanford University, Stanford, CA 94305, USA

Key Points:

- Deep neural network pickers can increase the efficiency of earthquake cataloging workflow.
- The sequence appears to be composed of two sub-sequences possibly triggered by different wells.
- Improved catalog reveals characteristic spatio-temporal seismicity patterns.

Corresponding author: Yongsoo Park, ysp@stanford.edu

Abstract

We revisited the June, 2010 - October, 2011 Guy-Greenbrier earthquake sequence in central Arkansas using PhaseNet, a deep neural network trained to pick P and S arrival times. We applied PhaseNet to continuous waveform data and used phase association and hypocenter relocation to locate nearly 90,000 events. Our catalog suggests that the sequence consists of two adjacent earthquake sequences on the same fault and that the second sequence may be associated with the wastewater disposal well to the west of the Guy-Greenbrier Fault, rather than the wells to the north and the east that were previously implicated. We find that each sequence is comprised of many small clusters that exhibit diffusion along the fault at shorter time scales. Our study demonstrates that machine learning based earthquake catalog development is now feasible and will yield new insights into earthquake behavior.

Plain Language Summary

Finding small earthquake signals from long duration continuous seismic data is a time consuming task, but machine learning algorithms have the potential to accelerate the workflow and improve the results. We reprocessed the seismic data from the area spanning Guy and Greenbrier in central Arkansas in 2010 and 2011 using a machine learning algorithm to re-examine this well-studied earthquake sequence, which is thought to be caused by injection of wastewater from uncoventional hydrocarbon production into deep disposal wells. Even using conservative post-processing steps, we were able to locate nearly 90,000 earthquake events. The improved catalog illuminates previously unseen aspects of this earthquake sequence that give new insights into its behavior.

1 Introduction

The Guy-Greenbrier sequence stretched from June, 2010 to October, 2011 in the region spanning Guy and Greenbrier, Arkansas and is thought to have been induced by some combination of hydraulic stimulation of horizontal production wells and injection of wastewater into deep disposal wells. Since the work published by Horton in 2012 (Horton, 2012), this sequence has become an important subject for induced seismicity studies (Horton, 2012; Llenos & Michael, 2013; Huang & Beroza, 2015; Huang et al., 2016; Ogwari et al., 2016; Ogwari & Horton, 2016; Yoon et al., 2017; Mousavi et al., 2017; Yehya et al., 2018).

Some of these studies have focused on improving the catalog using different algorithms and workflows. Ogwari and co-workers (Ogwari et al., 2016) used the short-time average/long-time average (STA/LTA) trigger for detection, manually picked P and S arrival times, and located 17,395 events from July 7, 2010 to October 20, 2010. From their improved catalog they concluded that seismicity was mostly correlated with the wastewater disposal well located close to the north end of the Guy-Greenbrier Fault. Yoon and co-workers (Yoon et al., 2017) applied the FAST algorithm (Yoon et al., 2015) and found over 10,000 events during the period from June 1, 2010 to August 31, 2010. They were able to locate 1,740 events, which revealed multiple event clusters from hydraulic fracturing operations as well as the initial stages of seismicity at the north end of the Guy-Greenbrier Fault.

While these studies provided new insight into the initial stages of the sequence, the activity over the remaining 12 months of the sequence received less attention. Huang and Beroza (Huang & Beroza, 2015) used single station template matching on continuous waveform from July, 2010 to October, 2011 and detected over 460,000 events. The detections in their study clearly showed two peaks of seismic activity: the first in October-November, 2010 and the second in February-March, 2011, however, the hypocenters of the detected events were undetermined.

Cataloging small earthquakes from long continuous data involves a trade-off between detecting all the events and avoiding false detections. Avoiding false positive detections is often done through manual inspection in a post-processing stage, and the number of waveforms to inspect can grow quite rapidly. Machine learning algorithms have the potential to play an important role in this application (Bergen et al., 2019). In particular, deep neural network arrival time pickers (Zhu & Beroza, 2018; Ross et al., 2018) have the potential to accelerate the front end of the seismicity analysis workflow by reducing the need for human arrival time picking. The robustness of these algorithms can reduce the number of false positives, which can reduce the need for analysts to hand tune parameters and inspect waveforms. In this study, we use the PhaseNet arrival time picker developed by Zhu and Beroza (Zhu & Beroza, 2018), which uses the U-Net architecture (Ronneberger et al., 2015) as trained on the Northern California earthquake catalog. We demonstrate how this tool can accelerate and improve the earthquake cataloging workflow. The improved catalog that results leads to new insights into this already well studied earthquake sequence.

2 Method

PhaseNet (Zhu & Beroza, 2018) takes a 3-component seismogram or a single channel vertical seismogram as input, and outputs the probability of each time step being a P arrival, an S arrival, or neither. The algorithm is designed such that the probability will peak at the arrival time of the phase. We use data from ten stations located near the Guy-Greenbrier Fault. Station WHAR was operational during the entire period from June 1, 2010 to October 31, 2011, while the other stations covered only a portion of the period (Table S1) resulting in a temporally and spatially variable network. Each component of the data was high pass filtered at 1 Hz and windowed into traces with 3,000 samples. We used an overlap of 1,500 samples to prevent earthquake signals being truncated at the edges. We removed duplicate picks in the post-processing step by tracking their timestamps and retained only the picks with probability 0.5 or higher. Traces containing time gaps were discarded. The approximate wall clock time for running the network on a month of continuous data from a single station was around 40 minutes on a single Intel Xeon CPU E5-2683V4 (2.10 GHz) hardware.

We associated the picks returned by the neural network by grid searching for a matching synthetic moveout calculated from the travel times, similar to the methods described in (Johnson et al., 1997; Zhang et al., 2019) using the velocity model in (Yoon et al., 2017). For efficient computation, we allowed a maximum separation of 20 seconds per event when forming possible moveouts from the picks, and used a lookup table for the travel times, which was built after discretizing the domain into blocks with latitude and longitude spacing of 0.004 degrees and depth spacing of 0.4 km. We allowed a difference between observed and synthetic travel time of up to 0.4 seconds and retained only the cases with at least 4 associated picks from at least 3 stations as candidate events. The number of events after association was 100,092. We used HYPOINVERSE-2000 (Klein, 2002) to locate each event independently and used the grid search solutions to initialize hypocenters. We discarded events with RMS travel time residual greater than 0.2 seconds, horizontal error of greater than 5 km, and depth error of greater than 5 km. This reduced the number of events to 96,191.

These initial locations placed the majority of the events on the Guy-Greenbrier Fault, with others forming small clusters that appeared to be a combination of natural seismicity, hydraulic fracturing operations, quarry blasts, and scatter due to the event being ei-

ther poorly located or a false positive. We separate these events into two groups: the on-fault group, which are spread along the Guy-Greenbrier Fault, and the off-fault group, which are more widely distributed, to facilitate double-difference relocation (Waldhauser & Ellsworth, 2000). The on-fault group was composed of the events within 2 km of the Guy-Greenbrier Fault and the remaining events were put into the off-fault group. The on-fault group was further separated into a group of well-constrained events and a group of poorly constrained events, based on the errors computed from HYPOINVERSE-2000. We used a horizontal error of 1 km and a depth error of 2 km for the separation.

We paired all events with the well-constrained events to compute arrival time differences by waveform cross-correlation. We bandpassed the data from 1 to 25 Hz and the windows for cross-correlation were set to 0.2 seconds before and 0.4 seconds after the P arrival, and 0.4 seconds before and 0.8 seconds after the S arrival, with shift length of 0.3 seconds. We set the search radius to 2 km when pairing two well-constrained events and to 5 km when pairing a poorly constrained event with a well-constrained event after setting the depths of all events to zero. The number of pairs was restricted to 100 when pairing each poorly constrained event with well-constrained events to prevent the cluster centroid from moving towards the locations of the poorly constrained events. We paired neighboring events that had at least 4 differential travel time observations from 3 stations with cross-correlation coefficient of 0.7 or above. The February 28, 2011 mainshock had enough phase arrival picks to determine the initial hypocenter but it could not be paired with other events using cross-correlation because the data was partially clipped. Therefore, we paired this event with 1,000 other events that were within 2 km radius and had highly confident picks (probability of 0.9 or greater). We passed the differential travel times to the HypoDD double-difference relocation algorithm (Waldhauser, 2001) and the group was treated as a single cluster. After relocation, the events that did not belong to the now-sharp Guy-Greenbrier Fault and the scattered events that were appended to the on-fault group that were not paired with other events were placed back to the off-fault group.

Most clusters and scattered events in the off-fault group had poor azimuthal station coverage, i.e., an azimuthal gap greater than 180 degrees. Rather than separating the events into well- and poorly constrained groups, we took a more conservative approach and only retained the events that had at least 5 other events within 1.5 km radius and that had at least 4 differential travel time observations from 3 stations with cross-correlation

coefficient of 0.7 or higher. The final number of events after the double-difference relocation was 86,657 for the on-fault group and 2,499 for the off-fault group, making the total count of 89,156. List of events are provided in Table S3 and the epicenters are plotted in Figure 1 along with the seismic stations, wastewater disposal wells, and production wells. The production wells are colored based on their completion date, which can either be the completion date of drilling or the date after hydraulic stimulation.

We estimated local magnitudes with station WHAR alone as 99 percent of the events had phase picks from this station. We used the distance calibration factors from (Yoon et al., 2017) on 1 Hz highpass filtered waveforms converted to standard Wood-Anderson response. We measured the average of the zero to peak amplitudes of the two horizontal components. We did not calculate magnitudes of the 866 events (fewer than 1% of the total) not picked by station WHAR, and used the previously reported magnitude (M 4.7) for the February 28, 2011 mainshock.

3 Evaluation of the Workflow

Monthly counts of P and S arrival time picks returned by the picker, and those eventually used for locating the events as well as the ratio between the two (yield) are listed in Table S2. The number of picks from station WHAR was the highest (P: 283,248, S: 280,331), but the overall yield was only around 0.3. The low yield is due to the limited number and relatively poorer performance of the other stations that were simultaneously in operation. There was a maximum of seven stations and an average of five during the study period. Because we required each event to have at least 4 phase picks from 3 stations during phase association, events that were missed by a few stations were not associated. This is especially apparent when comparing pre- and post- September, 2010 in Table S2 where introducing additional stations increased the yield substantially. Note that data quality from stations ARK1 and ARK2 was much lower than station WHAR, which is apparent in the relatively low number of picks over the same period of operation. More stations with high quality data would have greatly increased the yield from station WHAR and the total number of events in the catalog.

Figure 2 shows frequency-magnitude distribution of the events along the Guy-Greenbrier fault plotted per batch of 1,000 with magnitude bin size of 0.1. The batch before the February sequence, i.e., the distribution on the left to the vertical line at February 15, 2011,

contains 337 events and the last batch contains 457 events. To indicate an approximate level of magnitude of completeness (M_C) for the figure, we used the b-value stability criterion (Cao & Gao, 2002), where the b-values were calculated using the maximum likelihood estimation (Aki, 1965), and manually picked the cutoff magnitude that led to the first stable b-value as M_C. These are shown in solid line in Figure 2. Note that these are approximated values and are not intended for quantitative analysis, but rather to support the notion that our catalog is statistically homogeneous enough to make an unbiased interpretation.

4 The Case for Two Sequences

Figure 3(a) shows the evolution of seismicity along the Guy-Greenbrier Fault, i.e., the events colored in grey and the events that coincide with Well X (API: 03045102980000), as a function of time versus distance from point O along the dashed line in Figure 1. The sequence along the Guy-Greenbrier Fault is composed of two distinct sub-sequences that are separated from each other both in space and time. We refer to the two sub-sequences as the July sequence and the February sequence. Figure 4 shows the evolution of the July sequence, the initial stage of the February sequence, and the rest of the February sequence in separate plots based on the distance from point O in Figure 1 versus depth. The events that occurred in February 15, 2011, which is the start date of the February sequence, are plotted with filled circles in Figure 4(b). We plot events with magnitude 3 or greater with unfilled circles scaled by their estimated source radius assuming a constant stress drop of 9.47 MPa (Huang et al., 2016).

The early stages of the July sequence are well explained by previous studies (Ogwari et al., 2016; Ogwari & Horton, 2016; Mousavi et al., 2017) suggesting it was caused by injection at Well 1 and 5. However, the explanation for the February sequence and the time delay between the two sequences is less clear. The separation of the two sequences was observed in the study by Horton (Horton, 2012) and he hypothesized that the February sequence could have been influenced by the Enders Fault hydraulically connecting Well 2 and 5 with the Guy-Greenbrier Fault. Note that Well 2 is located to the west of the Guy-Greenbrier Fault and to the north of the Enders Fault (Figure 1) and was operating since April 2009 with a comparable injection rate to Well 1 (Well 1: 62663 $m^3/month$, Well 2: 54058 $m^3/month$) while the injection rate of Well 5 was much lower (19580 $m^3/month$). The events detected by Huang and Beroza (Huang & Beroza, 2015) also clearly showed

the seismically less active period between late December, 2010 and early February, 2011. However, they associated both sequences with Well 1 and 5 instead of suggesting an alternative explanation. Later, Yehya and coworkers (Yehya et al., 2018) again associated the February sequence to Well 1 and 5 but suggested that the time delay between the two sequences could be caused by the Enders Fault providing a barrier to pore pressure diffusion along the Guy-Greenbrier Fault.

The spatio-temporal evolution observed in our study suggests an alternative explanation. The initiation point of the February sequence was more than a kilometer south of the Enders Fault and spread bilaterally - north towards the Enders Fault and the July sequence, as well as to the south. This is displayed in Figure 3(b) and Figure 4(b) in two different views, and more explicitly in the supplementary animation (Movie S1). Moreover, the seismicity cluster CL1 in Figure 1 suggests that the medium between the Enders Fault and the Guy-Greenbrier Fault went through stress perturbation before the February sequence potentially due to the pore pressure diffusion from Well 2. Note that there are no production wells in the vicinity, which makes the possibility of these events being triggered by hydraulic fracturing less likely. We suggest that pressure from Well 2 could also have diffused to the Guy-Greenbrier Fault, but not necessarily through the Enders Fault, triggering the February sequence. Such remote triggering of seismicity is also proposed and a well-accepted mechanism in Oklahoma and Kansas (Keranen et al., 2014; Peterie et al., 2018).

Our observations also suggest that the July sequence effectively decayed before Wells 1 and 5 were shut down. The seismicity cluster near the north end that formed in early March, 2011 is likely to be associated with Well X where its reported date of the first treatment was February 28, 2011 with a completion date of March 7, 2011 (Figure 3).

Several clusters exterior to the Guy-Greenbrier Fault are also apparent in Figure 1. While the relative locations were improved by the double-difference algorithm, the absolute locations of most of these clusters remain uncertain due to the poor azimuthal station coverage. However, most clusters collocate with production wells both in space and time, based on the well completion date, as discussed by Yoon and coworkers (Yoon et al., 2017). Thus, it is likely that these clusters are associated with hydraulic fracturing operations. The clusters on the west side of Well 3 (annotated with CL2 in Figure 1) and to the northeast of the Guy-Greenbrier Fault (annotated with CL3 in Figure 1), how-

ever, do not collocate with any production wells in the vicinity. Similar to CL1, these could be associated with long-term injection of the nearby wastewater disposal wells, or to natural seismicity.

The depth versus distance plots in Figure 4 also exhibits multiple gaps in seismicity. The linear gap near the vertical line corresponding to the approximate intersection between the Guy-Greenbrier Fault and the Enders Fault in Figure 4(c) is especially notable. While this is spatially correlated with the Enders Fault, precise information of the fault geometry is required for confirmation.

5 Diffusion of Seismicity at Two Time Scales

The diffusivity of a seismicity front with respect to a point injection source or other reference point is an important metric for analyzing induced seismicity (Shapiro et al., 2002; Segall & Lu, 2015). The February sequence showed a smoothly migrating front in both directions. Approximating the diffusivity with respect to the initiation point of the February sequence using $r = \sqrt{4\pi Dt}$ yields a diffusivity of 2.4 m^2/s for the northern front and 1.6 m^2/s for the southern front (Figure 3(b)).

The overall sequence is comprised of a hierarchy of multiple smaller arc-shaped patterns of seismicity in space-time. These smaller seismicity patterns propagate at a somewhat faster rate over the fault than does the large-scale front. Two well-separated arc-structures that span the south end of the fault are shown in Figure 3(b) and their hypocenters are shown in 3(c) as examples. The implied diffusivity is correspondingly higher - 8 m^2/s in both instances. It is not necessarily clear what quantity is diffusing, with pore fluid, stress, and aseismic slip being among the possibilities. Regardless of the cause, observing such detailed features in the seismicity is only possible through the systematic cataloging of small earthquakes.

Yet another aspect of interest, which is most clearly revealed in the animation (Movie S1), is the propensity of parts of the fault to be illuminated by microearthquake activity multiple times. Most prominent are parts of the fault from 3-7.5 km along strike that were initially active in February, but were reactivated from March 22-23, and even more dramatically from April 7-8. Such behavior could occur if small events were driven by otherwise aseismic slip.

6 Conclusion

Through the case study of the Guy-Greenbrier seismic sequence, we demonstrate that machine-learning-based analysis of earthquake sequences is now possible. The PhaseNet deep neural network arrival time picker can accelerate the front end of earthquake catalog development that in this instance led to precise locations of almost 90,000 events. Our results suggest that the Guy-Greenbrier seismicity consisted of two sub-sequences, that the second sequence may have been triggered by a wastewater disposal well previously not implicated, and revealed diffusive patterns of seismicity at shorter time scales, and repeated illumination of large parts of the fault by seismicity.

Acknowledgments

This work is supported by the Stanford Center for Induced and Triggered Seismicity (SCITS) and the Department of Energy. Seismic data for stations ARK1, ARK2, ARK3, WHAR, X103, X201, X301, and X401 were downloaded from the Incorporated Research Institutions for Seismology (IRIS) at `http://ds.iris.edu/ds/` and data for stations Q201 and Q202 were obtained from P. Ogwari through S. M. Mousavi. Well information was obtained from the Arkansas Oil and Gas Commission (AOGC) at `http://www.aogc.state.ar.us/welldata/wells` and ENVERUS at `https://www.enverus.com`. Y. Park wants to thank C. E. Yoon for sharing her code scripts for local magnitude and differential travel time calculations.

References

Aki, K. (1965). Maximum likelihood estimate of b in the formula log n= a-bm and its confidence limits. *Bull. Earthq. Res. Inst., Tokyo Univ.*, *43*, 237–239.

Bergen, K. J., Johnson, P. A., Maarten, V., & Beroza, G. C. (2019). Machine learning for data-driven discovery in solid earth geoscience. *Science*, *363*(6433), eaau0323.

Cao, A., & Gao, S. S. (2002). Temporal variation of seismic b-values beneath northeastern japan island arc. *Geophysical research letters*, *29*(9), 48–1.

Horton, S. (2012). Disposal of hydrofracking waste fluid by injection into subsurface aquifers triggers earthquake swarm in central arkansas with potential for damaging earthquake. *Seismological Research Letters*, *83*(2), 250–260.

Huang, Y., & Beroza, G. C. (2015). Temporal variation in the magnitude-frequency

distribution during the guy-greenbrier earthquake sequence. *Geophysical Research Letters*, *42*(16), 6639–6646.

Huang, Y., Beroza, G. C., & Ellsworth, W. L. (2016). Stress drop estimates of potentially induced earthquakes in the guy-greenbrier sequence. *Journal of Geophysical Research: Solid Earth*, *121*(9), 6597–6607.

Johnson, C. E., Lindh, A., & Hirshorn, B. (1997). *Robust regional phase association.* US Department of the Interior, US Geological Survey.

Keranen, K. M., Weingarten, M., Abers, G. A., Bekins, B. A., & Ge, S. (2014). Sharp increase in central oklahoma seismicity since 2008 induced by massive wastewater injection. *Science*, *345*(6195), 448–451.

Klein, F. W. (2002). *User's guide to hypoinverse-2000, a fortran program to solve for earthquake locations and magnitudes* (Tech. Rep.). US Geological Survey.

Llenos, A. L., & Michael, A. J. (2013). Modeling earthquake rate changes in oklahoma and arkansas: Possible signatures of induced seismicity. *Bulletin of the Seismological Society of America*, *103*(5), 2850–2861.

Mousavi, S. M., Ogwari, P. O., Horton, S. P., & Langston, C. A. (2017). Spatio-temporal evolution of frequency-magnitude distribution and seismogenic index during initiation of induced seismicity at guy-greenbrier, arkansas. *Physics of the Earth and Planetary Interiors*, *267*, 53–66.

Ogwari, P. O., & Horton, S. (2016). Numerical model of pore-pressure diffusion associated with the initiation of the 2010–2011 guy–greenbrier, arkansas earthquakes. *Geofluids*, *16*(5), 954–970.

Ogwari, P. O., Horton, S. P., & Ausbrooks, S. (2016). Characteristics of induced/triggered earthquakes during the startup phase of the guy–greenbrier earthquake sequence in north–central arkansas. *Seismological Research Letters*, *87*(3), 620–630.

Peterie, S. L., Miller, R. D., Intfen, J. W., & Gonzales, J. B. (2018). Earthquakes in kansas induced by extremely far-field pressure diffusion. *Geophysical Research Letters*, *45*(3), 1395–1401.

Ronneberger, O., Fischer, P., & Brox, T. (2015). U-net: Convolutional networks for biomedical image segmentation. In *International conference on medical image computing and computer-assisted intervention* (pp. 234–241).

Ross, Z. E., Meier, M.-A., & Hauksson, E. (2018). P wave arrival picking and first-

motion polarity determination with deep learning. *Journal of Geophysical Research: Solid Earth*, *123*(6), 5120–5129.

Segall, P., & Lu, S. (2015). Injection-induced seismicity: Poroelastic and earthquake nucleation effects. *Journal of Geophysical Research: Solid Earth*, *120*(7), 5082–5103.

Shapiro, S. A., Rothert, E., Rath, V., & Rindschwentner, J. (2002). Characterization of fluid transport properties of reservoirs using induced microseismicity. *Geophysics*, *67*(1), 212–220.

Waldhauser, F. (2001). hypodd–a program to compute double-difference hypocenter locations.

Waldhauser, F., & Ellsworth, W. L. (2000). A double-difference earthquake location algorithm: Method and application to the northern hayward fault, california. *Bulletin of the Seismological Society of America*, *90*(6), 1353–1368.

Yehya, A., Yang, Z., & Rice, J. R. (2018). Effect of fault architecture and permeability evolution on response to fluid injection. *Journal of Geophysical Research: Solid Earth*, *123*(11), 9982–9997.

Yoon, C. E., Huang, Y., Ellsworth, W. L., & Beroza, G. C. (2017). Seismicity during the initial stages of the guy-greenbrier, arkansas, earthquake sequence. *Journal of Geophysical Research: Solid Earth*, *122*(11), 9253–9274.

Yoon, C. E., O'Reilly, O., Bergen, K. J., & Beroza, G. C. (2015). Earthquake detection through computationally efficient similarity search. *Science advances*, *1*(11), e1501057.

Zhang, M., Ellsworth, W. L., & Beroza, G. C. (2019). Rapid earthquake association and location. *Seismological Research Letters*, *90*(6), 2276–2284.

Zhu, W., & Beroza, G. C. (2018). Phasenet: a deep-neural-network-based seismic arrival-time picking method. *Geophysical Journal International*, *216*(1), 261–273.

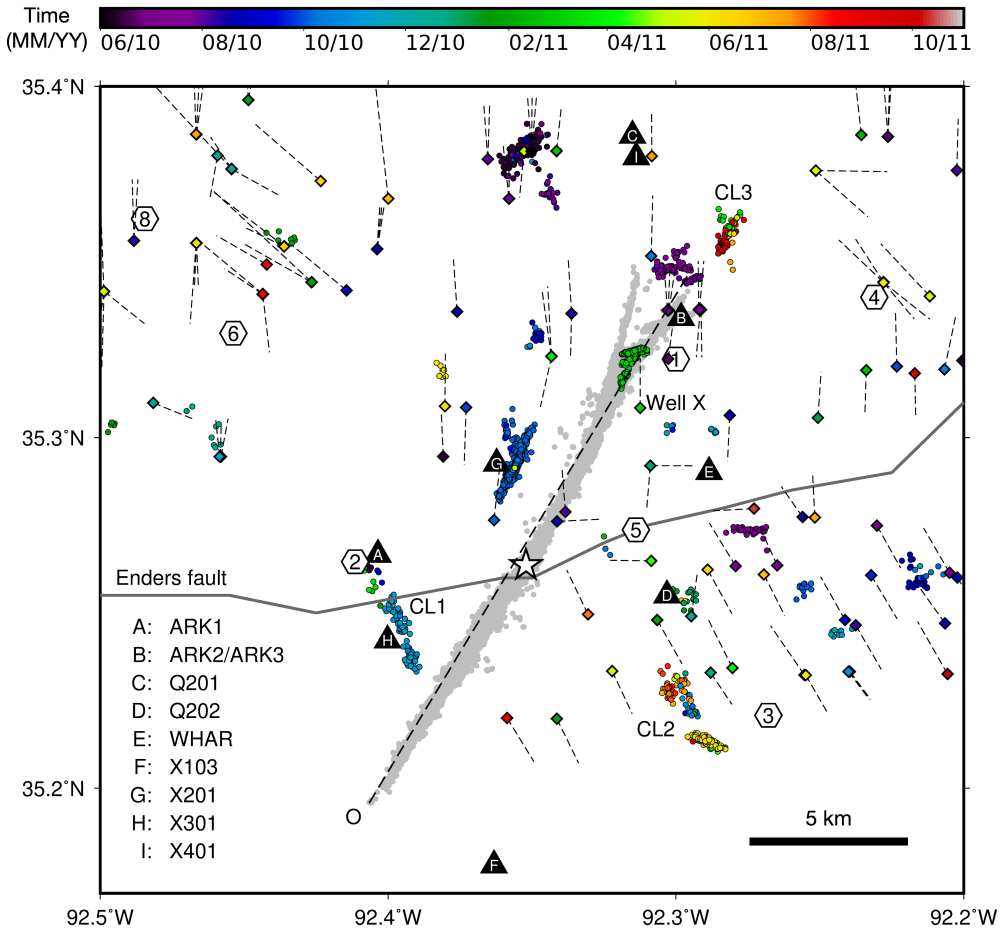

Figure 1. Epicenters of the 89,156 located events. Triangles are seismic stations, star is the February 28, 2011 mainshock, hexagons are wastewater disposal wells with well numbers based on Horton (Horton, 2012), and diamonds are production wells with each dashed line connecting the heel-toe. Events that are exterior to the Guy-Greenbrier Fault and the events that collocates with Well X (API: 03045102980000) in space and time are colored by their origin time. Production wells are colored by their completion date. See text for details.

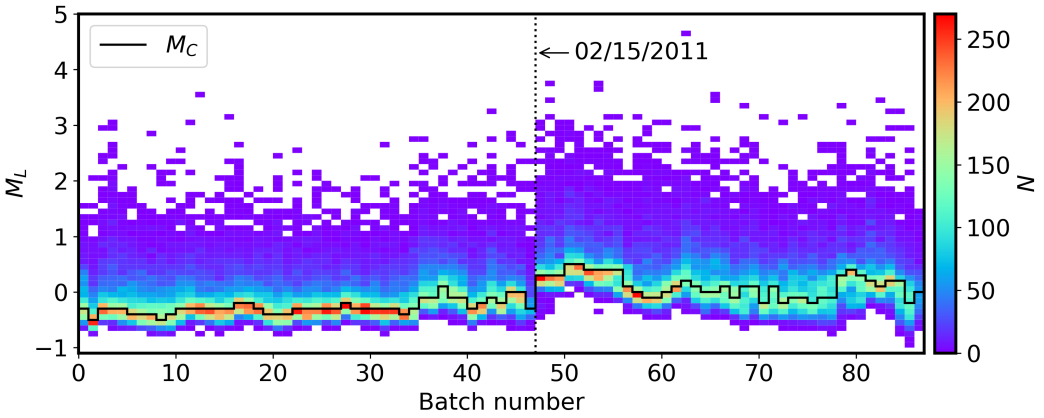

Figure 2. Frequency-magnitude distribution of the events along the Guy-Greenbrier Fault. Each batch contains 1,000 events except the batch before the February 15, 2011 line (337 events) and the last batch (457 events). The magnitude bin size was set to 0.1. Estimated magnitude of completeness (M_C) per batch is shown in solid line.

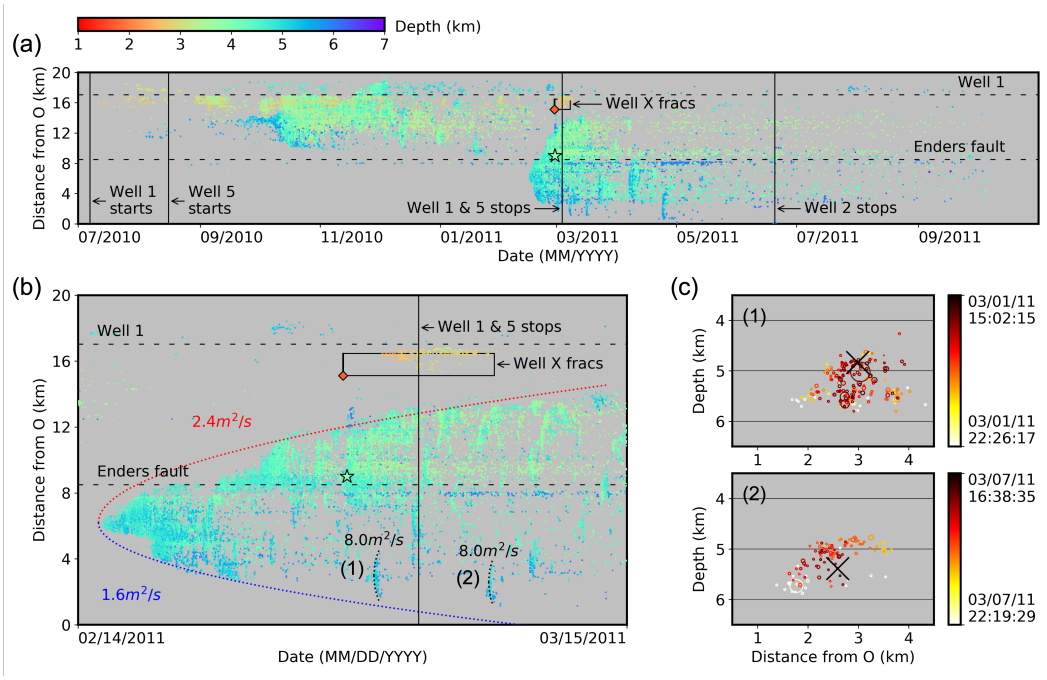

Figure 3. Events along the Guy-Greenbrier Fault plotted by their origin times versus the distance from point O in Figure 1 (a) from July 1, 2010 to October 31, 2011 and (b) from February 14, 2011 to March 14, 2011. Subplot (c) shows the hypocenters of the events forming the two arc-shaped structures in (b) scaled by their source radius. The first event in each plot is marked with $\times$. Numbers in (b) are approximated diffusivities for each seismicity front. See text for details.

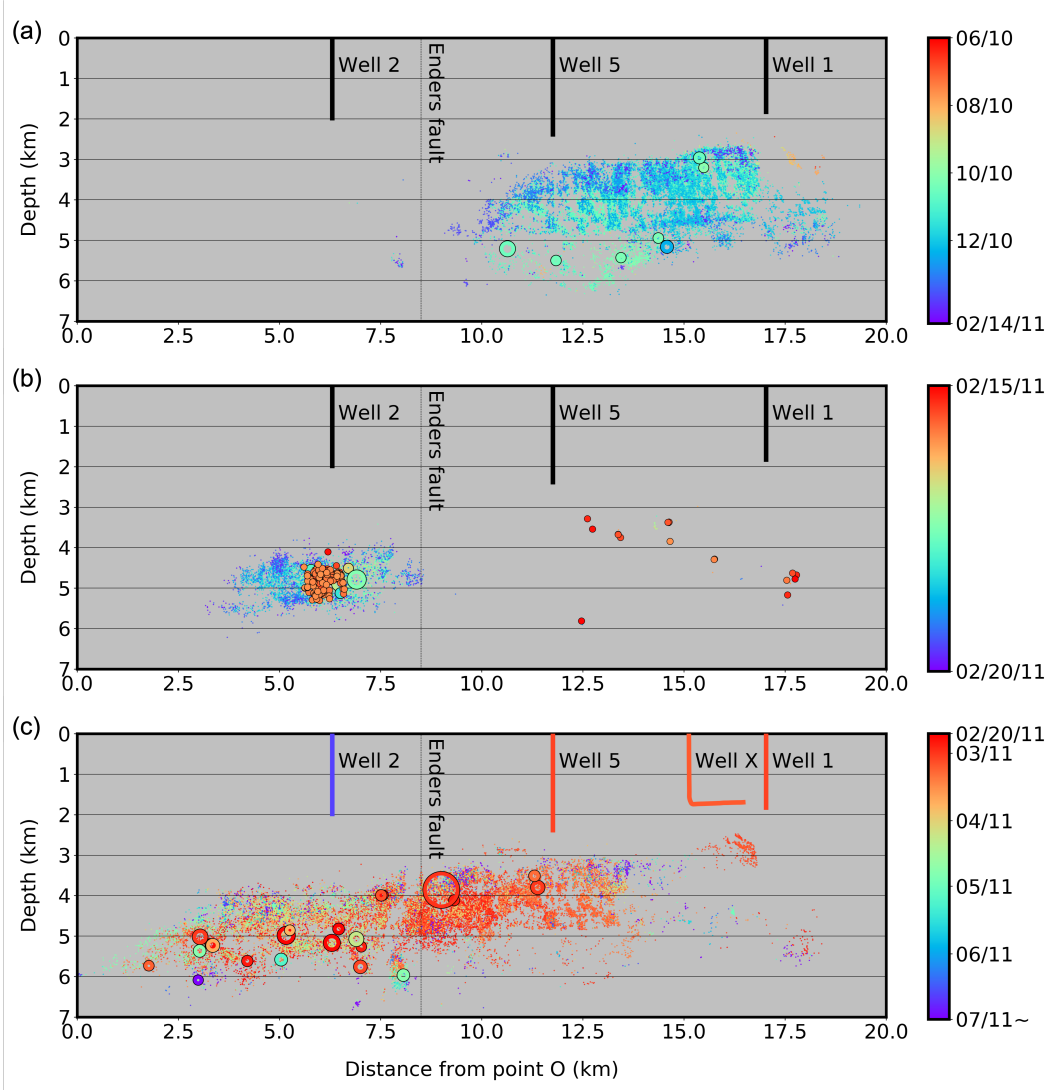

Figure 4. Events along the Guy-Greenbrier Fault plotted by the distance from point O in Figure 1 versus depth (a) from June 1, 2010 to February 14, 2011, (b) from February 15, 2011 to February 20, 2011, and (c) from February 20, 2011 to October 31, 2011. Events from February 15, 2011 (the initiation date of the February sequence) are plotted with filled circles in (b). Well 1, 2, and 5 are colored by their shutdown date and Well X is colored based on its completion date in (c). Events with magnitude 3 or greater are plotted in open circles scaled by their estimated source radius.